

ARTICLE

Open Access

Nano-encapsulation: overcoming conductivity limitations by growing MOF nanoparticles in meso-porous carbon enables high electrocatalytic performance

Krishnamoorthy Sathiyar¹, Asmita Dutta¹, Vered Marks¹, Ohad Fleker², Tomer Zidki¹, Richard D. Webster³ and Arie Borenstein¹

Abstract

Among the methods employed for carbon capture, the electroreduction of CO₂ offers both a reduction in CO₂ levels and the possibility of recycling it into commodity chemicals. However, the most efficient catalysts for this reaction are precious metals. To achieve cost-effective processes, other elements should be used. Transition-metal atoms coordinated with metal-organic frameworks (MOFs) exhibit high performance as electrocatalysts. However, the isolating natures of MOFs limit their utilization as electrocatalysts. In this study, we grew MOF nanoparticles inside hierarchically mesoporous carbon instead of mixing the MOFs with conductive carbon. The incorporated MOF nanoparticles showed improved properties compared with those of MOFs mixed with carbon, indicating strong electronic interactions in the composites. The encapsulated MOF nanoparticles demonstrated high electric conductivity while preserving their original crystallinity. When used as electrodes in CO₂ electroreduction, the MOFs exhibited a high electroactive coverage of 155 nmol cm⁻². Moreover, in a CO₂-saturated electrolyte, the composites exhibited excellent electrochemical performance, including a small onset potential (−0.31 V vs. RHE) and large reduction currents (−18 mA cm⁻² at −1.0 V); these were considerably higher than those usually reported for MOF-based materials except in CO electroreduction. Importantly, the composite produced valuable hydrogenated commodity chemicals, including formic acid.

Introduction

The increasing level of the greenhouse gas CO₂ in the atmosphere raises serious concerns for modern society^{1,2}. Long-running measurements have shown a steady increase in the mean atmospheric CO₂ concentration of 35% in the last 60 years (e.g., the famous Keeling curve)³. Decreasing the CO₂ concentration in the atmosphere has become a critical challenge for sustainable development and decoupling economic growth and CO₂ emissions.

CO₂ conversion into valuable chemicals offers the smallest ecological footprint at the highest resource utilization level⁴. The electrochemical carbon dioxide reduction reaction (CO₂RR) is attractive in terms of cost, availability, reaction conditions, and product separation feasibility^{5,6}. Importantly, the electrocatalytic reactions may result in different products, depending on many factors, including the catalyst, the solution, the applied potential, and time. Generally, at moderately negative potentials (up to −0.8 V vs. SHE), the predominant product is CO⁷. Therefore, lower onset potentials are required to generate more valuable products.

Many metals have been tested as cathode materials in electrocatalytic processes. Both experiments and theory

Correspondence: Arie Borenstein (arieb@ariel.ac.il)

¹Department of Chemical Sciences, Ariel University, Ariel, Israel

²Nesher Israeli Cement Enterprises, Ramla, Israel

Full list of author information is available at the end of the article

These authors contributed equally: Krishnamoorthy Sathiyar, Asmita Dutta

© The Author(s) 2023



Open Access This article is licensed under a Creative Commons Attribution 4.0 International License, which permits use, sharing, adaptation, distribution and reproduction in any medium or format, as long as you give appropriate credit to the original author(s) and the source, provide a link to the Creative Commons license, and indicate if changes were made. The images or other third party material in this article are included in the article's Creative Commons license, unless indicated otherwise in a credit line to the material. If material is not included in the article's Creative Commons license and your intended use is not permitted by statutory regulation or exceeds the permitted use, you will need to obtain permission directly from the copyright holder. To view a copy of this license, visit <http://creativecommons.org/licenses/by/4.0/>.

have proved that Cu is the only effective pure metal catalyst that effectively forms products beyond CO, namely, hydrocarbons and alcohols^{8,9}. The relatively weak energy for binding of CO to Cu allows the formation of the highly reduced carbon products. On the other hand, the copper shows adverse performance in terms of Faradaic efficiency (F.E., i.e., the ratio of charge utilized for the desired reaction out of total charge consumed in the system). In addition, Cu electrodes tend to generate wide ranges of reaction products with low selectivities¹⁰. In aqueous solutions, electrochemical recycling of CO₂ faces another challenge. The redox potentials for CO₂ reduction are similar to those of the hydrogen evolution reaction in aqueous solutions. Therefore, good selectivity of a CO₂ reduction catalyst is essential for achieving a highly efficient system.

Metal-organic frameworks (MOFs) have shown high compatibility and effectiveness in different applications in recent decades. MOFs are hybrid materials containing three well-differentiated sites to which catalytic functions can be allocated, namely, the metal component (d-band center), the organic linker (for example, cyanides (C-N)), and the pore space^{11,12}. MOFs exhibit excellent suitability as candidates for adsorption¹³, separation¹⁴, and reduction during catalyzed reactions^{15,16}. Their combined advantageous properties, i.e., large surface area, high porosity, and tunable pore size, provide promising results in electrocatalysis^{7,17}. In this regard, the advanced performance characteristics include smaller onset potentials¹⁸, stability¹⁹, and high Faradaic efficiency^{20,21}.

Although MOFs have many dominant advantages for the CO₂RR, they suffer from low intrinsic conductivity. Considerable effort has been devoted to improving the electrical conductivity of the material, with only limited success. Recent advanced techniques such as laser graphitization improved the material properties^{22,23}. The structural integrity of graphene was improved by patching carbon dots with laser irradiation to form 3D graphene with enhanced electrical conductivity^{24,25}. In approaching this challenge, researchers turned to pyrolyzing (also called carbonizing) MOFs to obtain metal atoms embedded in a conductive lattice^{19,26–28}. However, carbonized MOFs lack the unique electronic structure that supports catalytic capacity, thus severely diminishing the advantages of MOFs^{2,18,29}. To overcome this obstacle, MOF powders are commonly mixed with carbon black, micron-sized grained graphite particles, to enhance the overall conductivity of the electrode. Embedding carbon materials with non-conductive active materials is a known technique for improving conductivity^{30,31}. Nevertheless, this does not improve the intrinsic conductivity or performance.

A few years ago, research performed in our laboratory led to a MOF/carbon composite in which MOF nanoparticles were grown inside the pores of porous carbon.

These composites demonstrated excellent conductivity and improved electrical response without impairing the structural and chemical properties of the MOFs³². Cu-MOF-based catalysts have great potential for the electrochemical recycling of CO₂ into commodity chemicals because of their improved selectivities and high CO binding energies. The compositions of these MOFs with conductive and porous carbons may enhance their electric conductivities and solvent accessibilities, improve their stabilities, decrease onset potentials, and increase material loading.

Results and discussion

To demonstrate the advantages of supporting MOFs on a carbonaceous scaffold, we prepared HKUST-1 nanoparticles inside a porous activated carbon. HKUST-1 is a well-known Cu-based MOF material constructed of dimeric metal units connected by benzene-1,3,5-tricarboxylic acid (BTC) linkers. The MOF/carbon composite was prepared according to the method described previously³². The precursors of the MOF, namely, copper chloride and BTC, were separately introduced into the nanopores of activated carbon by continuously stirring the activated carbon particles in a BTC solution and then a copper chloride solution. A subsequent hydrothermal reaction resulted in the MOF nanoparticles (Fig. 1).

X-ray diffraction (XRD) was employed to characterize the crystal structure of the composite (Fig. 2a). Notably, the carbon matrix did not shield the XRD signals of the encapsulated MOFs. Moreover, HKUST-1 is known for its morphological sensitivity to synthetic conditions;³³ however, the porous carbon composition did not adversely affect the MOF crystallinity. The XRD pattern of the composite perfectly matched the pattern for MOFs synthesized from the carbon and also contained a broad peak centered at ~25°, corresponding to the (002) planes of graphitic segments in the carbon. At the proper MOF/carbon ratio of 1:3 (w/w), almost all of the MOFs were located inside the carbon pores, as indicated by SEM (Fig. S1). Due to the strong interactions of the MOF organic components with the aromatic rings of the host carbon, the originally nonconductive MOFs developed excellent lateral conductivity (up to 17.4 S/m) constituting an 85-fold increase compared to 0.2 S/m of the precursor HKUST-1 (Table 1). A simple mixture of the MOFs and carbon in the same mass ratio led to an 8.4-fold conductance improvement (1.69 S/m). Importantly, the composite maintained an extremely high surface area (940 m² g⁻¹). The surface area and pore size distribution of the composite are due to the combination of the two materials as a result of partial blockage of the mesopores of the activated carbon host by the MOF nanoparticles. Additionally, the sizes of the nanoparticles perfectly matched the sizes of the pores in which they were grown.

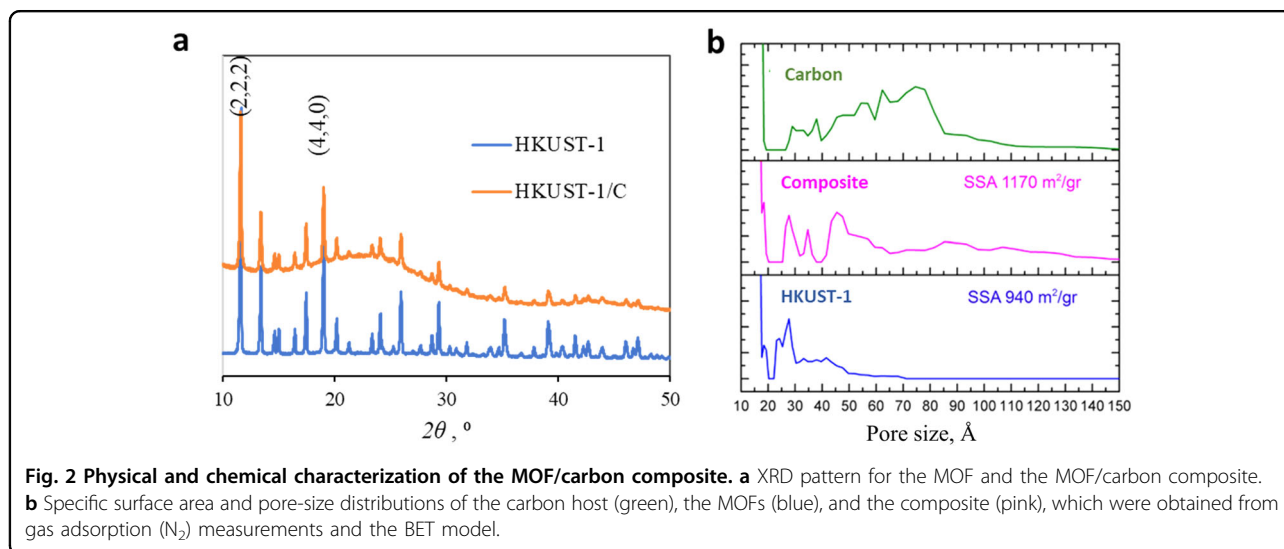
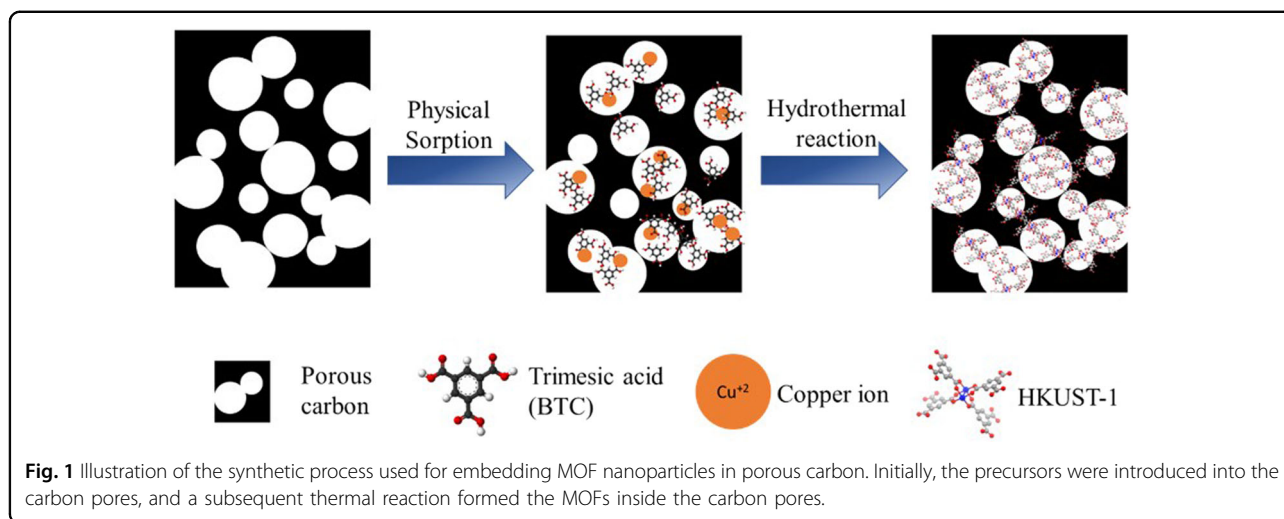
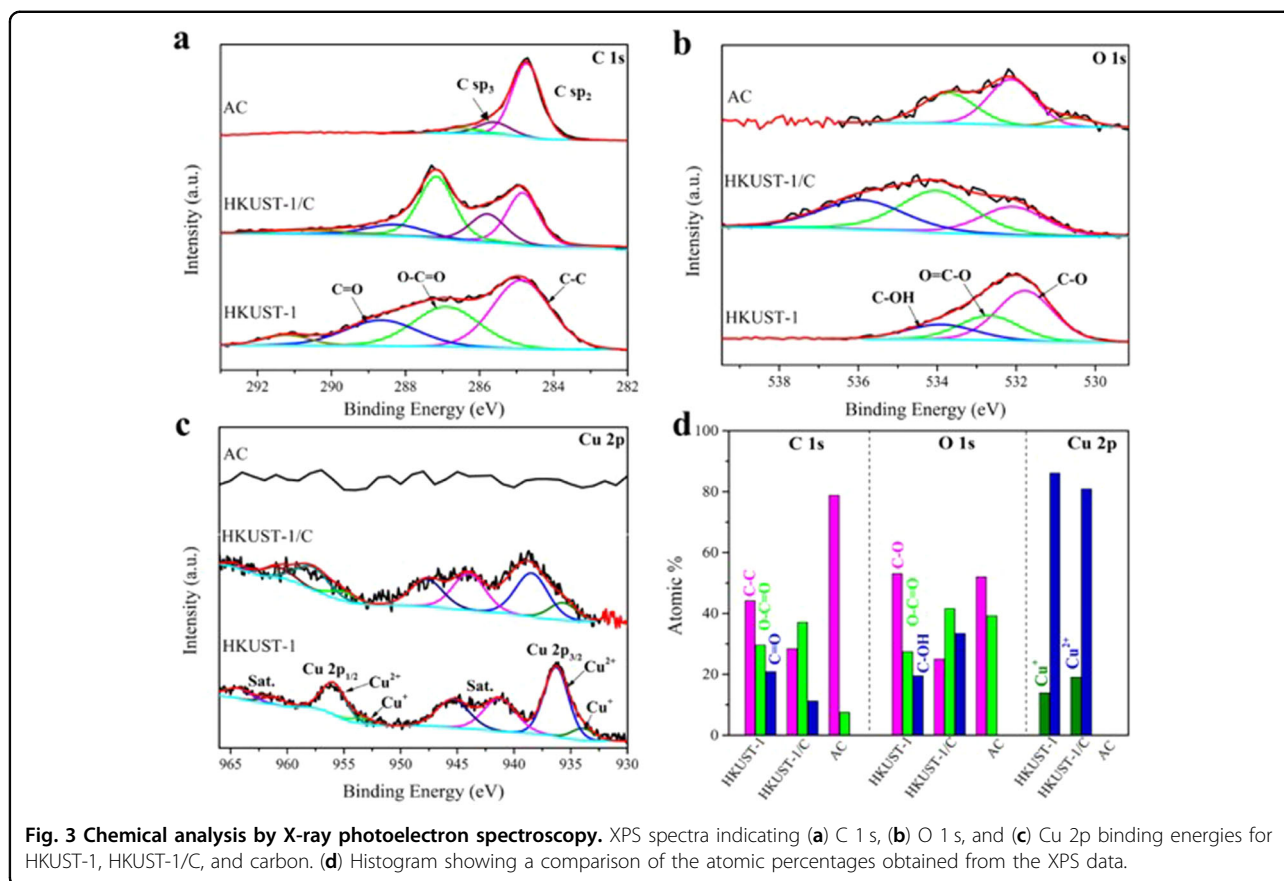


Table 1 Lateral electrical conductivities of HKUST-1/carbon composites with different MOF/carbon ratios, which indicate the significant advantages of our composition method compared to simple mixing of the MOFs with carbon.

Sample #	HKUST-1 content in sample	Composited with carbon ($S m^{-1}$)	Mixed with carbon ($S m^{-1}$)
1	Carbon	65	65
2	16%	17.2	1.69
3	23%	7.6	0.95
4	37%	0.2	0.09
5	HKUST-1	0.0003	0.0003

A large and accessible surface area is of great importance for electrochemical reactions, since it enables good accessibility of the reacting compounds (Fig. 2b; for isotherms, see Fig. S2).

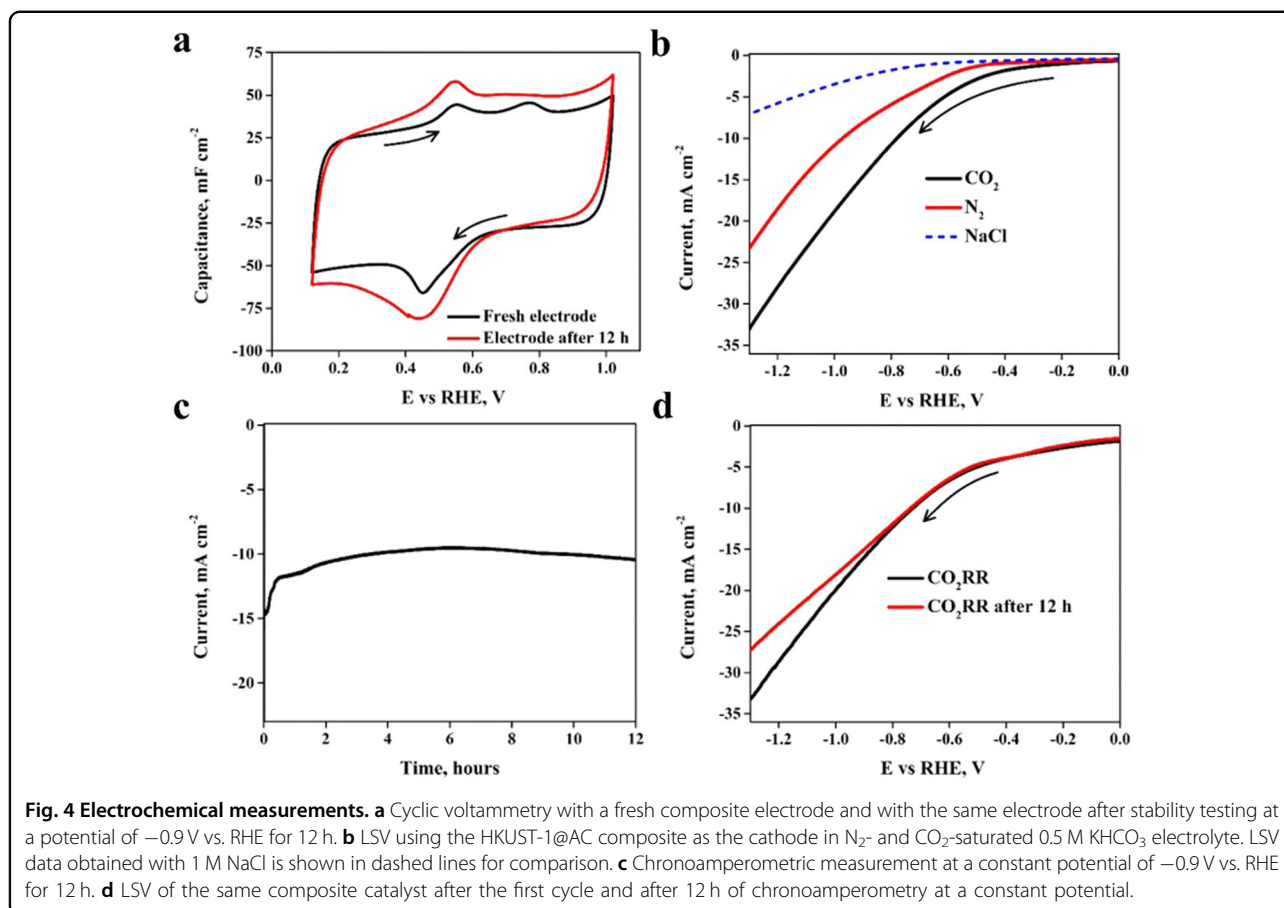
Thermal gravimetric analysis (TGA, Fig. S3) demonstrated the strong physical interactions between the MOFs and the carbon. The excellent adhesion of the MOFs on the carbon scaffold increased its thermal stability. Unmodified HKUST-1 lost approximately half of its original mass at $\sim 400^\circ C$, whereas this loss was obtained at a $50^\circ C$ higher temperature when it was incorporated into the carbon. Furthermore, the electronic interactions between the MOFs and carbon were previously identified by electron paramagnetic resonance (EPR) spectroscopy. The g-value of the unpaired Cu^{2+} electron in the composite was lower than that of the bare HKUST-1 (Fig. S4).



This shift toward the free-electron value (g -value of 2.0023) indicated that the Cu^{2+} unpaired electron in the composite had gained a higher level of mobility (less localized to the Cu atoms). A higher level of freedom for electrons originating from the metal center proved the conductivity of the surrounding carbon. The changes in electronic structure imposed by the composite structure may have affected the catalytic properties of HKUST-1, including the yields, onset potentials and catalytic mechanisms, resulting in various products. Moreover, by analyzing the different g -values recorded for the composite, we simulated the average size of the MOF nanoparticles (considering a HKUST-1 unit cell with a diameter of 0.9 nm). Interestingly, the mean diameter of the MOF nanoparticles was 6 nm and perfectly matched the average pore size of the carbon host, as determined by gas adsorption measurements (Fig. 2b)³².

X-ray photoelectron spectroscopy (XPS) provided additional insight into the electronic state of the modified MOFs. XPS analyzes the binding energies of valence electrons in atoms and is therefore sensitive to the oxidation states of the elements. The full survey spectra, including peaks for C 1s, O 1s, and Cu 2p binding energies, are presented in Fig. S5. The spectrum for the activated carbon indicated 96% carbon and no detectable

copper (Table S1). On the other hand, the spectra of the MOFs indicated 68.4% carbon, 29.8% oxygen, and 2.3% copper, similar to the atomic ratio in HKUST-1. Predictably, the spectrum of the composite was a combination of those for its two precursors. It contained one-quarter of the Cu compared to the MOFs, which was in good agreement with the MOF/carbon ratio in the composition. The spectra were normalized with the C 1s peak at 284.8 eV. Deconvolution of the C 1s peak revealed the chemical interactions between atoms. The C 1s spectrum of the activated carbon indicated mainly carbon-carbon bonding (79%). On the other hand, the MOF spectrum showed 60% oxygen-bonded carbon atoms, indicative of the carboxyl groups of the BTC linkers (Fig. 3a and Table S2). Interestingly, the binding energies of the corresponding peaks shifted in each spectrum. While the binding energy of the C-O peak in HKUST-1 was 287.3 eV, the binding energy of the composite was shifted toward a higher binding energy of 288.27 eV. This was closer to the peak found for the activated carbon at 288.65 eV. The shift of the C 1s peak revealed a higher oxidation state for the carbon atoms in the composite compared to those in the original MOF. The deconvoluted O 1s peak followed the same trend, in which the second peak, which originated from O-C moieties, was



shifted from 532.6 eV in HKUST-1 to 533.7 eV in the composite (Fig. 3b). The most significant shift was found in the Cu 2p spectrum (Fig. 3c). Importantly, this peak was absent from the spectrum for activated carbon and enables direct tracking of the changes in the electronic state of the MOFs after composition. The fitted XPS data for Cu confirmed the presence of both Cu^+ and Cu^{2+} ; peaks for binding energies of 933.9 and 953.3 eV corresponded to the $2p_{3/2}$ and $2p_{1/2}$ states Cu(I), respectively, and the peaks at 936.2 and 956.0 eV were associated with the same electronic states for Cu(II)^{34–37}. All copper peaks were shifted to higher binding energies, which was attributed to the strong interaction between HKUST-1 and the activated carbon. Here, the peak for Cu^{2+} was upshifted from 936.2 eV in the original MOFs to 938.0 eV in the composite. The peak shifts resulted from the electronic interactions of the MOFs with the hosting carbon, and this supported the interpretations of the EPR data that were reconfirmed by the electrochemical activity. When encapsulating the MOF guest, the more oxidized activated carbon acted as an electron withdrawer and applied a partial positive charge on the MOFs, both at the chelating oxygen atoms and the copper centers. The electronic interactions ultimately led to higher electron

mobility and electrical conductivity. A comparison of the atomic ratios obtained from XPS data is shown in a histogram (Fig. 3d). Further analyses of the XPS spectra can be found in the supporting information.

To evaluate the electrocatalytic capability of HKUST-1/C, the composite was used as the cathode in a three-electrode cell. A conductive ink comprising HKUST-1/C, carbon black (CB) as a conducting agent, and Nafion as an ion-conducting binder was prepared and drop-cast on carbon cloth electrodes. Cyclic voltammetry (CV) studies using the electrode in a CO_2 -saturated KHCO_3 solution showed a widely spaced $\text{Cu}^+/\text{Cu}^{2+}$ oxidation/reduction couple with peaks at 0.76 and 0.45 V vs. RHE, respectively (Fig. 4a). An important parameter for high surface area composite catalysts is the degree of electroactive coverage, i.e., the number of active sites available in the material for electrochemical reactions. The CV reduction peak at -0.05 V vs. Ag/AgCl was used to measure the concentration of electroactive copper centers (Fig. S6). Integrating the reduction wave produced with a CV scan rate of 10 mV s^{-1} revealed that 0.015 Coulombs participated in the electrochemical reaction (Fig. S6). Considering that this reaction involves only single electron transfer, approximately 155 nmol of Cu^{2+} sites were exposed to the

Table 2 Performance of different MOF-based cathodes for CO₂ electroreduction.

Cathode	<i>J</i> , mA cm ⁻²	<i>E</i> V vs. SHE	Electrochemical coverage nmoles cm ⁻²	Main product	Reference
MOF-545Fe/CB	1.2	-0.6	3	CO	49
Al ₂ (OH) ₂ TCCP-Co	1	-1.7	18	CO	19
COF-367-Co	3.3	-0.67	2	CO	50
MOF-1992/CB	16.6	-0.63	270	CO	29
CuPc	2.8	-1.6	N.A. ^c	C ₂ H ₄	18
Fe-TPP	3	-1.0	0.1	CO	20
HKUST-1/carbon	18	-1.0	155	HCOO⁻	This work

^c - could not be extracted from the paper.

electrolyte solution and actively participated in the electrochemical reduction reaction. This is approximately 18% of the Cu atoms in the total electrode. The high electroactive coverage indicated exceptionally high exposure of the metal centers to the electrolyte, among the highest ever reported for MOF-based cathodes (Table 2 and Table S3).

Linear sweep voltammetry (LSV) was employed to study the cathode performance in the CO₂ electroreduction reaction. The selection of a proper electrolytic solution is crucial for enabling the reaction. As bicarbonate is well known to produce CO₂, a potassium bicarbonate solution was used as the electrolyte for the CO₂ reduction reaction as per the previous studies^{38–43}. When polarized to negative potentials, the HKUST-1/carbon composite demonstrated an exceptionally high increase in the negative current density, starting at an onset potential of -0.31 V (Fig. 4b, black line). Moreover, at -1.0 V vs. RHE, the LSV with the MOF/carbon exhibited a current density of -18 mA cm⁻² in the presence of CO₂. This was considerably higher than the current densities usually reported for MOF-based catalysts, except with CO electrocatalysis (Table 2 and Table S3). The excellent performance resulted from the extremely high electrochemical coverage of the MOFs and the electrical activity originating from amalgamation with the carbon host. The gaseous CO₂ reacted with water to form carbonic acid, H₂CO₃, which allowed the dissolution of more CO₂. The resulting H₂CO₃ was in equilibrium with bicarbonate (HCO₃⁻), which in turn was in equilibrium with carbonate (CO₃²⁻). Under our reaction conditions with a neutral pH, carbonate was protonated to form bicarbonate. Because of this, the CO₂-saturated solution had more bicarbonate anions undergoing the CO₂ reduction process. To ensure that the cathodic current originated from CO₂ reduction (CO₂ + 2H⁺ + 2e⁻ → CO + H₂O) and not from the hydrogen evolution reaction (HER, 2H⁺ + 2e⁻ → H₂), the electrodes were tested in a similar apparatus with a NaCl

solution used as the supporting electrolyte. In this CO₂-free electrolyte solution, the onset potential was shifted down to -0.52 V. Presumably, in the absence of carbonate ions, the reduction was associated with the HER, proving high selectivity for the catalyst. (Fig. 4b, blue dashed line). LSV was run at lower scan rates (2 mVs⁻¹), and the identical results confirmed that the source of the current was Faradaic and not capacitive (Fig. S7). These excellent results resulted from the unique chemical structure of the composite material. To prove the superiority of the composite, we tested all of the individual components electrochemically. Fig. S8a shows the LSV results for the HKUST-1 MOF, activated carbon, and a copper salt loaded on activated carbon. Both the currents and the overpotentials observed for the nanocomposite outperformed those observed for all of the separate components. EIS measurements showed the smaller resistivity of the composite compared to that of every individual component (Fig. S8b and Table S4).

The stability of the catalyst during prolonged operation is a major challenge in electrocatalytic processes²⁸. To evaluate the stability of electrocatalysis, we applied a constant potential (*E* = -0.9 V vs. RHE) to a MOF/carbon composite electrode in a CO₂-saturated solution (Fig. 4c). An average current density of -10.56 mA cm⁻² was measured at the initial stage of the reaction, and -11.85 mA cm⁻² was measured after 12 h. The sustained current density indicated excellent chemical stability. The remarkable stability should be attributed to the stability of the carbon host. Durability was also tested with repeated LSV and CV experiments after 12 h of chronoamperometry (Fig. 4a, d). Both measurements revealed almost identical responses for the fresh electrodes and the electrodes held at constant potential for 12 h. We also tested the stability of the electrode at acidic and basic pHs (3, 6 and 12), and Fig. S9 shows comparisons of chronoamperometry measurements lasting 12 h with galvanostatic measurements in normal bicarbonate

solution (pH 8.25). The reduction currents in the acidic solutions were similar, and those in the basic solution (pH = 12) were significantly lower. Prolonged stability tests prove the excellent stabilities of the composite electrodes over a large range of pH values. XRD measurements were performed before and after the chronoamperometry tests (Fig. S10). The results showed that the MOF/carbon composite retained its stable structure. These results were promising and encourage further studies of the activities and selectivities of MOF/carbon composites used as catalysts for the CO₂RR.

To make CO₂ reduction economically feasible, the products of the process must be valuable chemicals. It is worth noting that many studies have measured CO production and calculated the Faradaic efficiency for CO production, which is not a commodity chemical. In this study, we examined the formation of more highly reduced (hydrogenated) species; therefore, the production identification required NMR spectra. To identify the products of the reaction, the electrolyte solution used for the CO₂RR was collected from the reactor after 0.5 h, 2 h, 3 h, 5 h, and 10 h. The products were analyzed by H-NMR spectroscopy and quantified using maleic acid as the internal standard. Formic acid was identified as the main product via ¹H NMR spectrometry (Fig. 5). Importantly, products were observed even in the first sample taken after 30 min. The amount of each product varied during the 10 h of reaction. A peak at $\delta = 8.3$ ppm was attributed to formic acid. Two additional peaks near $\delta = 3.0$ were observed after the initial stages of the reaction. One was attributed to the central methylene (CH₂) group in malonic acid, HOOC = OCH₂C = OOH. We could not confirm the origin of the other peak near $\delta = 3.0$. We tried adding malonic

acid into the NMR tube containing the sample from CO₂ reduction (Fig. S11). The malonic acid showed a new peak, which indicated that the product was not malonic acid. Notably, the concentration of formic acid increased for the first three hours and decreased when the reaction continued for 12 h (Fig. S12). Interestingly, this decline in peak intensity after 3 h of reaction implied a second electrochemical reaction involved reduction of this initial product. It should be noted that when products were left in the reactor cell and subjected to low potentials, more highly reduced products may result;⁴⁴ earlier studies showed situations where products were seemingly lost from the reaction solution, and this was exacerbated by performing the reactions at low concentrations⁴⁵. Moreover, different potentials resulted in various products (Fig. 6a). The Faradaic efficiencies for formation of formic acid and hydrogen gas at different potentials are displayed in Fig. 6b. More formic acid was formed at lower potential, and less was observed with a higher potential because of competition from the hydrogen evolution reaction. This showed that CO₂ electroreduction predominantly occurs at a low potential at -0.3 V vs. RHE. Although CO is a common product in carbon dioxide reduction, after applying several potentials to the electrode material, we were unable to identify CO as a product of CO₂ reduction. The absence of CO product was confirmed by FTIR and electrochemical CO stripping tests (Figs S13, S14). CO-free product mixtures have been reported for many other studies using copper in electrocatalytic reductions^{46–48}.

Based on the products identified by NMR, we can propose a reduction mechanism that results in formic acid as the main product. This mechanism is based on multiple recent publications describing the use of a similar copper-based catalyst and formation of similar products^{20,44,45}. A plausible mechanism for the HKUST-1/C composite is shown in Fig. 7. In the initial reaction stages, the CO₂ contained in the electrolyte is adsorbed on the copper center and, under a negative potential, it is reduced to the CO₂^{•-} radical ion at the HKUST-1/C surface. The adsorbed CO₂^{•-} binds at the active sites on the catalyst surface and reacts with a proton to form a carboxyl radical (COOH) intermediate, which results in the formation of formic acid.

Conclusions

This work shows the high efficiency of a composite produced from the well-studied MOF HKUST-1 and activated carbon as an electrocatalyst for CO₂ electroreduction. To enable the use of MOFs in electrochemical applications, conductivity must first be established in naturally occurring materials. To achieve this conductivity, HKUST-1 nanoparticles were grown inside a conductive porous carbon. The strong interactions originating from π - π bonds between the aromatic linkers and

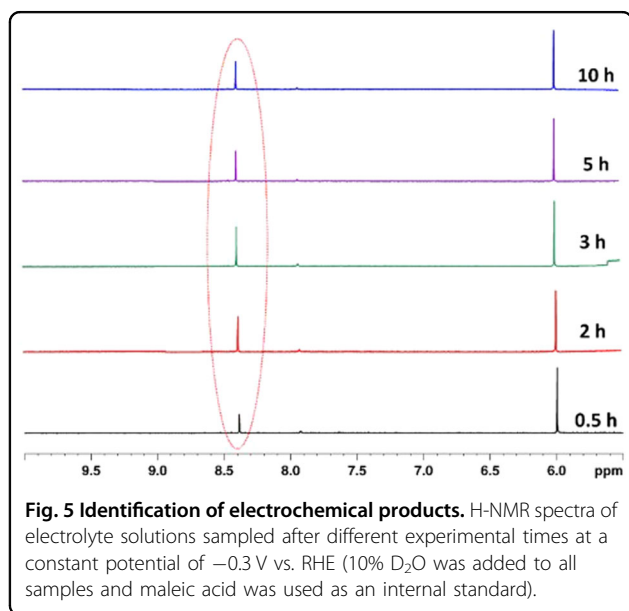
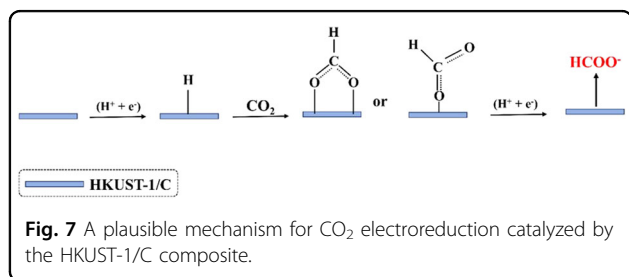
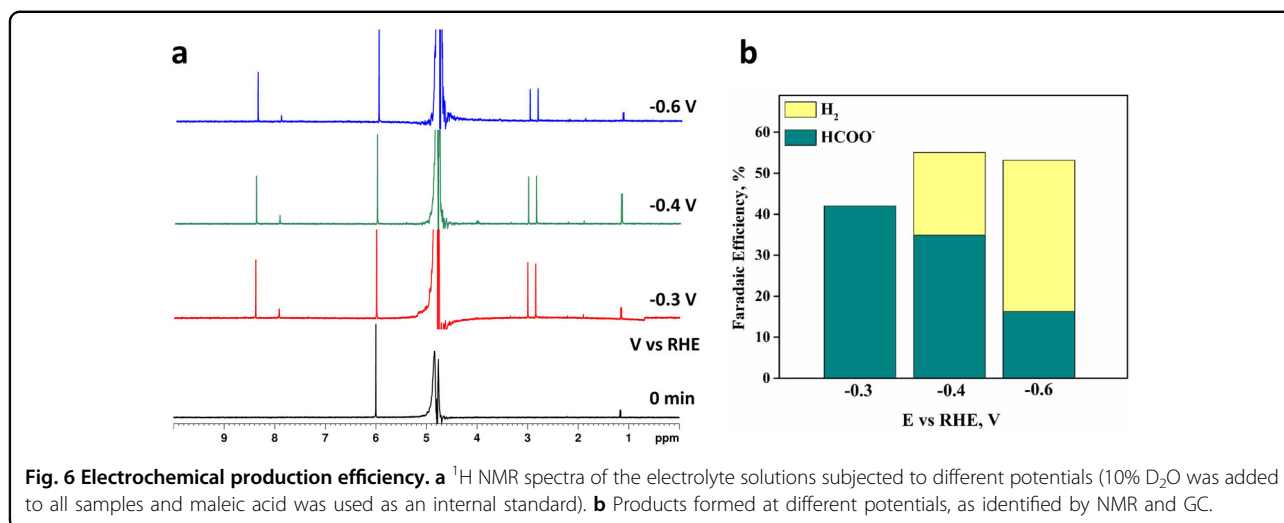


Fig. 5 Identification of electrochemical products. H-NMR spectra of electrolyte solutions sampled after different experimental times at a constant potential of -0.3 V vs. RHE (10% D₂O was added to all samples and maleic acid was used as an internal standard).



the graphitic carbon induced high lateral conductivity of up to 17.2 S m^{-1} for the composite. Moreover, an EPR study of the unpaired electrons on the Cu atoms revealed that the induced conductivity influenced the metal centers. Importantly, the conductivity achieved by the composite did not impact the crystal structure of the MOFs, as observed by XRD. Electrochemical studies revealed a high electroactive coverage of 155 nmol cm^{-2} . When operated in a CO_2 -saturated aqueous solution, the composite electrode exhibited excellent electrocatalytic performance. The onset potential for carbon dioxide electroreduction was -0.31 V vs. RHE, and the reduction current density at -1.0 V was -18 mA cm^{-2} , which may be the largest reduction current density ever reported, except for CO reduction. In addition, the composite stabilized the active material, and after 12 h of constant operation, the electrochemical response showed minor changes. The main product observed via ^1H -NMR was formic acid. These excellent results suggested the effectiveness of the composition method in allowing nonconductive MOFs to participate in electrochemical processes.

Experimental section

MOF/carbon composite synthesis

The synthesis of the MOF/carbon composite was described elsewhere³². The activated carbon used in this

research was obtained from Energy2, USA. HKUST-1/carbon composites were prepared by suspending 250 mg of oven-dried activated carbon in 10 mL of a dimethylformamide (DMF) solution of H_3BTC (103 mg , $4.9 \times 10^{-4} \text{ mol}$). The suspension was stirred at room temperature for several hours. $\text{Cu}(\text{OAc})_2 \cdot \text{H}_2\text{O}$ (147 mg , $7.3 \times 10^{-4} \text{ mol}$, 1.5 equiv. with respect to H_3BTC) was added, and the mixture was stirred for another 2 h at room temperature. The mixture was held overnight in an oven at 40°C in an autoclave. The resulting suspensions were centrifuged and decanted. Subsequently, the solid precipitate was washed with 15 mL of DMF. These washing cycles involving centrifuging and decanting were repeated three times. The resulting solid powders were suspended in acetone (5 mL) overnight and dried on a rotary evaporator. The dried samples were placed in an oven at 40°C and gradually heated to 150°C ($1^\circ\text{C}/\text{min}$) for approximately 4 h. The prepared composites were stored under an inert atmosphere. To compare our results with those from recent work, we also prepared HKUST-1/carbon mixtures by mixing appropriate quantities of HKUST-1 and AC. The obtained mixtures had the same HKUST-1/carbon ratios.

Gas adsorption measurements

Gas adsorption was measured using an Autosorb-1 MP (Quantachrome) system. The specific surface area was calculated using the Brunauer–Emmett–Teller (BET) model. The MOF was activated (solvent removal) by drying under a high vacuum of $1.5 \cdot 10^{-3} \text{ bar}$ at 150°C for 12 h before the surface area measurements.

Powder X-ray diffraction (PXRD)

Spectra were recorded using a Bruker AXS D8 Advance XRD. The MOF was activated (solvent removal) by drying under a high vacuum of $1.5 \cdot 10^{-3} \text{ bar}$ at 150°C for 12 h before XRD measurements.

X-ray photoelectron spectroscopy (XPS)

The XPS data were obtained with an (XPS/AES) ESCALAB 250 ultrahigh vacuum (1×10^{-9} bar) apparatus equipped with an Al-K α X-ray source and a monochromator. The measured spectra were calibrated relative to the C 1s peak at 284.6 eV. The survey spectra were analyzed with a pass energy (PE) of 150 eV, and the high energy resolution was realized with a PE of 20 eV.

Composite electrodes for electrochemical characterization

Electrodes were prepared by mixing the composite powder (active mass – MOF/carbon) with 5% Nafion as a binder and 5% carbon black serving as a conducting agent. While encapsulation of the MOF inside the carbon improved the intrinsic conductivity of the active material, the role of the conducting agent was to improve the conductivity between particles and bridge gaps in the electrode film. The ink was coated on a carbon cloth. The average active mass weight was 1.40 mg for a 1 cm² electrode.

Electrochemical measurements

For all experiments, 0.5 M potassium bicarbonate was used as the electrolyte. Prior to electrochemical testing, the electrolyte was saturated with CO₂. A standard three-electrode setup was employed with a platinum counter electrode and a Ag/AgCl reference electrode. These experiments were carried out with potentiostat/galvanostat computerized instruments from Bio-Logic Inc, France.

Cyclic voltammetry: The electrolyte solution was sparged for 15 min with N₂ or CO₂. The scan rate was 10 mV/s within the presented electrochemical potential windows. **Chronopotentiometry:** The electrolyte solution in the working compartment was sparged for 10 min with N₂ or CO₂. The applied potential was –0.3 V vs. RHE, based on the optimal performance of the cobalt phthalocyanine catalyst at that potential. The chronoamperograms were corrected for uncompensated resistance. The current density at $E = -0.3$ V vs. SHE was averaged from three independent MOF-1992/CB electrodes, and the standard deviation was used as the error.

Faradaic efficiency was calculated as

$$FE = n * F * Z / A * t$$

where $n = 2$ for a two-electron reaction, $F = 96485$ C/mol, Z = number of moles of formic acid produced, A is the measured current, and t is the time.

The conductivity measurements were conducted with two copper portals distanced 1 centimeter apart and pressed on the composite film. We measured the lateral conductivity rather than the bulk conductivity since it is difficult to determine the thickness of the electrode, and

cross-sectional microscope images showed that the thickness varied considerably (from ~0.8 to 2 micrometers).

More experimental and instrumental details can be found in the supplementary information.

Author details

¹Department of Chemical Sciences, Ariel University, Ariel, Israel. ²Nesher Israeli Cement Enterprises, Ramla, Israel. ³Division of Chemistry & Biological Chemistry, School of Physical and Mathematical Sciences, Nanyang Technological University, Singapore, Singapore

Author contributions

K.S. and A.D.- Sample preparation, analysis and electrochemical measurements. Manuscript writing. A.F.- Model and concept development, consultation. T.Z. and R.W.- Research planning, consultation. Manuscript review. A.B.- Supervising, conceptualization.

Conflict of interest

The authors declare no competing interests.

Publisher's note

Springer Nature remains neutral with regard to jurisdictional claims in published maps and institutional affiliations.

Supplementary information The online version contains supplementary material available at <https://doi.org/10.1038/s41427-022-00459-4>.

Received: 22 August 2022 Revised: 26 November 2022 Accepted: 29 November 2022.

Published online: 31 March 2023

References

- Al-Rowaili, F. N., Jamal, A., Ba Shammakh, M. S. & Rana, A. A Review on Recent Advances for Electrochemical Reduction of Carbon Dioxide to Methanol Using Metal-Organic Framework (MOF) and Non-MOF Catalysts: Challenges and Future Prospects. *ACS Sustain. Chem. Eng.* **6**, 15895–15914 (2018).
- Gong, Y. et al. Regulating the Coordination Environment of MOF-Templated Single-Atom Nickel Electrocatalysts for Boosting CO₂ Reduction. *Angew. Chem.* **132**, 2727–2731 (2020).
- Kasting, J. F. & Ackerman, T. P. Climatic consequences of very high carbon dioxide levels in the earth's early atmosphere. *Science* **234**, 1383–1385 (1986).
- Perathoner, S. & Centi, G. CO₂ recycling: A key strategy to introduce green energy in the chemical production chain. *ChemSusChem* **7**, 1274–1282 (2014).
- Poh, H. L., Sofer, Z., Luxa, J. & Pumera, M. Transition metal-depleted graphenes for electrochemical applications via reduction of CO₂ by lithium. *Small* **10**, 1529–1535 (2014).
- Khezri, B., Fisher, A. C. & Pumera, M. CO₂ reduction: The quest for electrocatalytic materials. *J. Mater. Chem. A* **5**, 8230–8246 (2017).
- Albo, J. et al. Copper-Based Metal–Organic Porous Materials for CO₂ Electrocatalytic Reduction to Alcohols. *ChemSusChem* **10**, 1100–1109 (2017).
- Bagger, A., Ju, W., Varela, A. S., Strasser, P. & Rossmeisl, J. Electrochemical CO₂ Reduction: A Classification Problem. *ChemPhysChem* **18**, 3266–3273 (2017).
- Dinh, C. T. et al. CO₂ electroreduction to ethylene via hydroxide-mediated copper catalysis at an abrupt interface. *Science* **360**, 783–787 (2018).
- Kuhl, K. P., Cave, E. R., Abram, D. N. & Jaramillo, T. F. New insights into the electrochemical reduction of carbon dioxide on metallic copper surfaces. *Energy Environ. Sci.* **5**, 7050–7059 (2012).
- Zhang, J., Vukmirovic, M. B., Xu, Y., Mavrikakis, M. & Adzic, R. R. Controlling the Catalytic Activity of Platinum-Monolayer Electrocatalysts for Oxygen Reduction with Different Substrates. *Angew. Chem.* **117**, 2170–2173 (2005).
- Deng, T. et al. Atom-Pair Catalysts Supported by N-Doped Graphene for the Nitrogen Reduction Reaction: D-Band Center-Based Descriptor. *J. Phys. Chem. Lett.* **11**, 6320–6329 (2020).
- Jiang, Z.-R. et al. Coating sponge with a hydrophobic porous coordination polymer containing a low-energy CF₃-decorated surface for continuous pumping recovery of an oil spill from water. *NPG Asia Mater.* **8**, e253 (2016).

14. Qian, Q. et al. MOF-Based Membranes for Gas Separations. *Chem. Rev.* **120**, 8161–8266 (2020).
15. Morozan, A. & Jaouen, F. Metal organic frameworks for electrochemical applications. *Energy Environ. Sci.* **5**, 9269 (2012).
16. Wu, M. et al. A Facile Activation Strategy for an MOF-Derived Metal-Free Oxygen Reduction Reaction Catalyst: Direct Access to Optimized Pore Structure and Nitrogen Species. *ACS Catal.* **7**, 6082–6088 (2017).
17. Yi, F.-Y. et al. Metal-Organic Frameworks and Their Composites: Synthesis and Electrochemical Applications. *Small Methods* **1**, 1700187 (2017).
18. Kusama, S., Saito, T., Hashiba, H., Sakai, A. & Yotsuhashi, S. Crystalline Copper(II) Phthalocyanine Catalysts for Electrochemical Reduction of Carbon Dioxide in Aqueous Media. *ACS Catal.* **7**, 8382–8385 (2017).
19. Kornienko, N. et al. Metal-Organic Frameworks for Electrocatalytic Reduction of Carbon Dioxide. *J. Am. Chem. Soc.* **137**, 14129–14135 (2015).
20. Hod, I. et al. Fe-Porphyrin-Based Metal-Organic Framework Films as High-Surface Concentration, Heterogeneous Catalysts for Electrochemical Reduction of CO₂. *ACS Catal.* **5**, 6302–6309 (2015).
21. Nam, D. H. et al. Metal-Organic Frameworks Mediate Cu Coordination for Selective CO₂ Electroreduction. *J. Am. Chem. Soc.* **140**, 11378–11386 (2018).
22. Dutta, A., Sathiyar, K., Sharon, D. & Borenstein, A. Laser induced incorporation of CNTs in graphene electrodes improves flexibility and conductivity. *FlatChem* **33**, 100378 (2022).
23. Yadav Kumar, M. & Borenstein, A. Is precarbonization necessary for effective laser graphitization? *Carbon* **199**, 208–214 (2022).
24. Strauss, V. et al. Patching laser-reduced graphene oxide with carbon nanodots. *Nanoscale* **11**, 12712–12719 (2019).
25. Borenstein, A., Strauss, V., Kowal, M. D., Anderson, M. & Kaner, R. B. Laser-Assisted Lattice Recovery of Graphene by Carbon Nanodot Incorporation. *Small* **15**, 1904918 (2019).
26. Varela, A. S. et al. Metal-Doped Nitrogenated Carbon as an Efficient Catalyst for Direct CO₂ Electroreduction to CO and Hydrocarbons. *Angew. Chem.* **127**, 10908–10912 (2015).
27. Shen, K., Chen, X., Chen, J. & Li, Y. Development of MOF-Derived Carbon-Based Nanomaterials for Efficient Catalysis. *ACS Catal.* **6**, 5887–5903 (2016).
28. Qiao, J., Liu, Y., Hong, F. & Zhang, J. A review of catalysts for the electroreduction of carbon dioxide to produce low-carbon fuels. *Chemical Society Reviews* **43**, (2014).
29. Matheu, R. et al. Three-Dimensional Phthalocyanine Metal-Catecholates for High Electrochemical Carbon Dioxide Reduction. *J. Am. Chem. Soc.* **141**, 17081–17085 (2019).
30. Dutta, A. et al. Surface modifications of carbon nanodots reveal the chemical source of their bright fluorescence. *Nanoscale Adv.* **3**, 716–724 (2021).
31. Kumar, V. B. et al. Activated Carbon Modified with Carbon Nanodots as Novel Electrode Material for Supercapacitors. *J. Phys. Chem. C.* **120**, 13406–13413 (2016).
32. Fleker, O. et al. Preparation and Properties of Metal Organic Framework/Activated Carbon Composite Materials. *Langmuir* **32**, 4935–4944 (2016).
33. Lee, Y. R., Kim, J. & Ahn, W. S. Synthesis of metal-organic frameworks: A mini review. *Korean J. Chem. Eng.* **30**, 1667–1680 (2013).
34. Zhang, J., Su, C., Xie, X., Liu, P. & Huo, M. E. Enhanced visible light photocatalytic degradation of dyes in aqueous solution activated by HKUST-1: performance and mechanism. *RSC Adv.* **10**, 37028–37034 (2020).
35. Chen, C. et al. Synthesis of Hierarchically Structured Hybrid Materials by Controlled Self-Assembly of Metal-Organic Framework with Mesoporous Silica for CO₂ Adsorption. *ACS Appl. Mater. Interfaces* **9**, 23060–23071 (2017).
36. Wang, Y. et al. Synthesis of porous Cu₂O/CuO cages using Cu-based metal-organic frameworks as templates and their gas-sensing properties. *J. Mater. Chem. A* **3**, 12796–12803 (2015).
37. Qiao, Y. et al. Construction of novel Ag/HKUST-1/g-C₃N₄ towards enhanced photocatalytic activity for the degradation of pollutants under visible light. *RSC Adv.* **9**, 41591–41602 (2019).
38. Tan, X. et al. J. Restructuring of Cu₂O to Cu₂O@Cu-Metal-Organic Frameworks for Selective Electrochemical Reduction of CO₂. *ACS Appl. Mater. Interfaces* **11**, 9904–9910 (2019).
39. Cao, S.-M. et al. Nitrogen-rich metal-organic framework mediated Cu-N-C composite catalysts for the electrochemical reduction of CO₂. *J. Energy Chem.* **54**, 555–563 (2021).
40. Li, D. et al. MOF-Derived Cu₂O/Cu Nanospheres Anchored in Nitrogen-Doped Hollow Porous Carbon Framework for Increasing the Selectivity and Activity of Electrochemical CO₂ to-Formate Conversion. *ACS Appl. Mater. Interfaces* **12**, 7030–7037 (2020).
41. Liu, J. et al. Metal-Organic-Frameworks-Derived Cu/Cu₂O Catalyst with Ultra-high Current Density for Continuous-Flow CO₂ Electroreduction. *ACS Sustain. Chem. Eng.* **7**, 15739–15746 (2019).
42. Zhao, K., Liu, Y., Quan, X., Chen, S. & Yu, H. CO₂ Electroreduction at Low Overpotential on Oxide-Derived Cu/Carbons Fabricated from Metal Organic Framework. *ACS Appl. Mater. Interfaces* **9**, 5302–5311 (2017).
43. Kim, M. K., Kim, H. J., Lim, H., Kwon, Y. & Jeong, H. M. Metal-organic framework-mediated strategy for enhanced methane production on copper nanoparticles in electrochemical CO₂ reduction. *Electrochim. Acta* **306**, 28–34 (2019).
44. Bondue, C. J., Calle-Vallejo, F., Figueiredo, M. C. & Koper, M. T. M. Structural principles to steer the selectivity of the electrocatalytic reduction of aliphatic ketones on platinum. *Nat. Catal.* **2**, 243–250 (2019).
45. Budanovic, M., Urbančok, D., Er, J. Y. H., Tessensohn, M. E. & Webster, R. D. Experimental Reasons for the Variable Efficiencies of Organic Electrocatalysts Used for Converting Carbon Dioxide to Methanol. *ChemElectroChem* **8**, 2075–2086 (2021).
46. Albo, J. et al. Copper-Based Metal-Organic Porous Materials for CO₂ Electrocatalytic Reduction to Alcohols. *ChemSusChem* **10**, 1100–1109 (2017).
47. Hwang, S.-M. et al. Investigation on Electroreduction of CO₂ to Formic Acid Using Cu₃(BTC)₂ Metal-Organic Framework (Cu-MOF) and Graphene Oxide. *ACS Omega* **5**, 23919–23930 (2020).
48. Gupta, K., Bersani, M. & Darr, J. A. Highly efficient electro-reduction of CO₂ to formic acid by nano-copper. *J. Mater. Chem. A* **4**, 13786–13794 (2016).
49. Dong, B. X. et al. Electrochemical Reduction of CO₂ to CO by a Heterogeneous Catalyst of Fe Porphyrin-Based Metal-Organic Framework. *ACS Appl. Energy Mater.* **1**, 4662–4669 (2018).
50. Lin, S. et al. Covalent organic frameworks comprising cobalt porphyrins for catalytic CO₂ reduction in water. *Science* **349**, 1208–1213 (2015).